Physical Interpretation of Flow and Heat Transfer in Preswirl Systems

Paul Lewis
e-mail: p.r.lewis@bath.ac.uk

Mike Wilson
e-mail: m.wilson@bath.ac.uk

Gary Lock
e-mail: g.d.lock@bath.ac.uk

J. Michael Owen
e-mail: j.m.owen@bath.ac.uk

University of Bath,
Bath BA2 7AY, UK

This paper compares heat transfer measurements from a preswirl rotor–stator experiment with three-dimensional (3D) steady-state results from a commercial computational fluid dynamics (CFD) code. The measured distribution of Nusselt number on the rotor surface was obtained from a scaled model of a gas turbine rotor–stator system, where the flow structure is representative of that found in an engine. Computations were carried out using a coupled multigrid Reynolds-averaged Navier-Stokes (RANS) solver with a high Reynolds number k-ε/k-ω turbulence model. Previous work has identified three parameters governing heat transfer: rotational Reynolds number (Re_ϕ)*, preswirl ratio* (β_p)*, and the turbulent flow parameter* (λ_T)*. For this study rotational Reynolds numbers are in the range* $0.8\times10^6<\mathrm{Re}_\phi<1.2\times10^6$*. The turbulent flow parameter and preswirl ratios varied between* $0.12<\lambda_T<0.38$ *and* $0.5<\beta_p<1.5$*, which are comparable to values that occur in industrial gas turbines. Two performance parameters have been calculated: the adiabatic effectiveness for the system,* $\Theta_{b,\mathrm{ad}}$*, and the discharge coefficient for the receiver holes,* C_D*. The computations show that, although* $\Theta_{b,\mathrm{ad}}$ *increases monotonically as* β_p *increases, there is a critical value of* β_p *at which* C_D *is a maximum. At high coolant flow rates, computations have predicted peaks in heat transfer at the radius of the preswirl nozzles. These were discovered during earlier experiments and are associated with the impingement of the preswirl flow on the rotor disk. At lower flow rates, the heat transfer is controlled by boundary-layer effects. The Nusselt number on the rotating disk increases as either* Re_ϕ *or* λ_T *increases, and is axisymmetric except in the region of the receiver holes, where significant two-dimensional variations are observed. The computed velocity field is used to explain the heat transfer distributions observed in the experiments. The regions of peak heat transfer around the receiver holes are a consequence of the route taken by the flow. Two routes have been identified: "direct," whereby flow forms a stream tube between the inlet and outlet; and "indirect," whereby flow mixes with the rotating core of fluid.* [DOI: 10.1115/1.2436572]

1 Introduction

The blade-cooling air in gas turbines is usually supplied to the rotating high-pressure blades by stationary preswirl nozzles. The cooling air is swirled, which reduces the work done by the rotating turbine disk in accelerating the air to the disk speed. This in turn reduces the total temperature of the air entering the receiver holes in the disk. A simplified diagram of the so-called direct transfer preswirl system is shown in Fig. 1.

The designer is interested in calculating the pressure drop and cooling effectiveness of the preswirl system. There is also a need to understand the heat transfer between the cooling air and the turbine disk, particularly the possible creation of local nonuniform temperatures in the metal that could lead to large thermal stresses.

Meierhofer and Franklin [1], who were the first to measure the effect of preswirl on the temperature drop in a direct-transfer system, showed that swirling the air could significantly reduce the total temperature in the receiver holes of a turbine disk. El-Oun and Owen [2] developed a theoretical model for the so-called adiabatic effectiveness, $\Theta_{b,\mathrm{ad}}$, based on the Reynolds analogy. The model, which was in good agreement with the temperatures measured on their rotating-disk rig, showed that $T_{t,b}$, the total temperature in the receiver holes, decreased monotonically as β_p, the preswirl ratio, increased even when β_p was significantly greater than unity.

Geis et al. [3] made measurements of the adiabatic effectiveness, which showed that the measured values of $T_{t,b}$ were significantly higher than the values predicted from their ideal model. (It should be pointed out that their preswirl ratio was based on isentropic values rather than on measurements.) Chew et al. [4] made numerical simulations of both the "Karlsruhe rig," used by Geis et al., and a "Sussex preswirl rig." The computations were in good agreement with the results of both rigs, and the low adiabatic effectiveness of the Karlsruhe rig was attributed to the geometry of the preswirl chamber; in particular, the Karlsruhe rig had a much larger stator area, which reduced the effective swirl ratio and consequently reduced the effectiveness.

Chew et al. [4] and Farzaneh-Gord et al. [5] independently derived theoretical models for the adiabatic effectiveness of a direct-transfer system, taking account of the moment on the stator. (These models predict lower values of $\Theta_{b,\mathrm{ad}}$ than that of Karabay et al. [6], who based their model on a cover-plate system in which the preswirl air flows radially outward between two rotating disks.)

Popp et al. [7] carried out a CFD analysis of a cover-plate system, computing the temperature drop and the discharge coefficients for different geometries. They showed that C_D, the discharge coefficient for the receiver holes, became a maximum when the relative tangential velocity was close to zero. This effect

Contributed by the International Gas Turbine Institute of ASME for publication in the JOURNAL OF ENGINEERING FOR GAS TURBINES AND POWER. Manuscript received July 19, 2006; final manuscript received July 20, 2006. Review conducted by Dilip R. Ballal. Paper presented at the ASME Turbo Expo 2006: Land, Sea and Air (GT2006), Barcelona, Spain, May 8–11, 2006. Paper No. GT2006-90132.

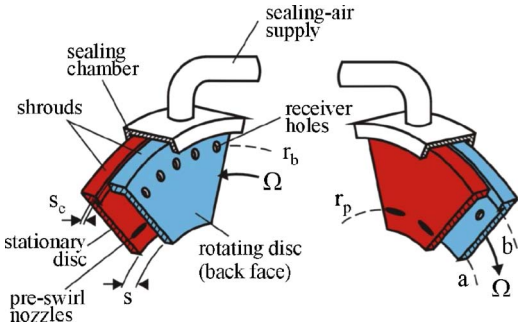

Fig. 1 Schematic diagram of test section

was confirmed experimentally by Dittmann et al. [8] who were the first to measure the discharge coefficients in a direct-transfer system.

Yan et al. [9] measured the discharge coefficients for the receiver holes of a direct-transfer system for a range of rotational speeds and flow rates. For $\beta_1 < 1$ (where β_1 is the measured swirl ratio upstream of the receiver holes) C_D increased monotonically as β_1 increased from $\beta_1 \approx 0.3$ to 0.9. They also found, as did Popp et al., that C_D depends on the ratio of the area of the receiver holes to that of the nozzles; for a given value of the preswirl ratio, β_p, C_D increases as the area ratio decreases. (It should be noted that, owing to a printer's error, the wrong figures were printed in Ref. [9]; the correct figures are given in Ref. [10]).

Heat transfer in a direct transfer rig was studied experimentally and computationally by Wilson et al. [11] using fluxmeters to determine the local Nusselt numbers. Their axisymmetric CFD results gave reasonable predictions of the velocity and temperature in the core but underpredicted the measured Nusselt numbers.

Numerous experimenters have used thermochromic liquid crystal (TLC) to determine heat transfer coefficients on purpose-built test sections. A common technique is to solve Fourier's transient conduction equation to calculate h for a semi-infinite solid exposed to a step change in air temperature. As it is virtually impossible to achieve a step change in the air temperature of preswirl rigs, Newton et al. [12] developed the so-called "slow transient" technique. Lock et al. [13,10] used this technique to measure the local Nusselt numbers, on the rotating disk of a direct-transfer rig, for a range of rotational speeds, flow rates, and preswirl ratios. The measurements showed that Nu was virtually axisymmetric except near the receiver holes, where large variations occurred. They also found that there were two flow regimes: at the larger preswirl flow rates, inertial effects dominated and the flow impinged on the rotating disk creating a peak in Nu; at the smaller flow rates, viscous effects dominated and boundary-layer flow controlled the heat transfer.

In this paper, a commercial three-dimensional (3D) CFD code is used to compute the flow and heat transfer in the "Bath rig" used by Lock et al. The computations are compared with measured values of the discharge coefficients, with theoretical values of adiabatic effectiveness and with measured local Nusselt numbers. In particular, the computations are used to give a physical insight into the complex flow and heat transfer that occurs in these direct-transfer preswirl systems.

2 Governing Parameters

Owen and Rogers [14] showed that, for a rotating cavity, the turbulent flow structure depends on only two nondimensional parameters: the inlet swirl ratio, β_p, and the turbulent flow parameter, λ_T. These are defined as

$$\beta_p = \frac{v_{\phi,p}}{\Omega r_p} \tag{1}$$

and

$$\lambda_T = c_w \, \mathrm{Re}_\phi^{-0.8} \tag{2}$$

where

$$c_w = \frac{\dot{m}_p}{\mu b} \tag{3}$$

and

$$\mathrm{Re}_\phi = \frac{\rho \Omega b^2}{\mu} \tag{4}$$

The value $\lambda_T = 0.22$ corresponds to the flow rate entrained by a disk rotating in an infinite environment, the so-called free disk. For turbine-blade cooling systems, $\lambda_T \approx 0.4$ and $\beta_p \approx 1$.

For the Bath rig (described in Sec. 3) it follows that

$$\beta_p = \frac{C}{N} \frac{c_w}{\mathrm{Re}_\phi} = \frac{C}{N} \frac{\lambda_T}{\mathrm{Re}_\phi^{0.2}} \tag{5}$$

where C is a geometric constant given by

$$C = \frac{4b^3 \cos\theta}{\pi d^2 r_p} \tag{6}$$

It can be seen that the preswirl ratio is not independently variable: it depends upon N, the number of preswirl nozzles, and upon λ_T and Re_ϕ. In the experiments of Yan et al. [9], two values of N were used: $N = 12$ and 24. In the experiments discussed below, $N = 24$.

The Bath rig uses a simplified engine geometry, and tests were conducted at representative values of β_p and λ_T, thereby producing flow structures typical of those found in engines. However, in engines Re_ϕ is on the order of 10^7, which is an order of magnitude greater than that achievable in the rig. As the heat transfer depends strongly on Re_ϕ, as well as on β_p and λ_T, the rig Nusselt numbers will be much smaller than those found in engines. This is discussed further in Sec. 6.

3 Experimental Method

Experimental results were produced by Yan et al. [9] and Lock et al. [13,10] using the "slow transient" TLC technique described by Newton et al. [12]. The salient points of the experimental method are presented here for convenience and a section of the experimental rig is illustrated in Fig. 1.

The rotor is a transparent polycarbonate disk with a radius of 0.216 m, allowing optical access to the wheel space. The disk has 60 circular receiver holes with centers at a disk radius of 0.200 m. To reduce heat transfer from the air inside the receiver holes, the holes are filled with Rohacell (low-conductivity foam) bushes producing an effective receiver hole diameter of 8.0 mm. The disk has a thickness of 10 mm, and the receiver holes, which have a length to diameter ratio of 1.25, vent directly into the laboratory. A shroud of carbon fiber surrounds the rim of the disk and rotates with it. A section of the rotor surface inside the wheelspace is painted with thermochromic liquid crystal.

The stator is also a polycarbonate disk, which is mounted onto an aluminum disk. The gap between the rotor and stator is 11 mm ($G = 0.051$), and the clearance between the rotating and stationary shrouds is 1 mm. The air pressure in the wheel space is balanced by sealing air to restrict leakage or ingress. The preswirl nozzles comprise 24 circular holes, of 7.1 mm diameter, drilled at an angle of 20 deg to the tangential direction and at a radius of 160 mm. A stationary Rohacell hub forms the inner boundary of the wheel space at a radius of 0.145 m.

The radial variation of pressure and tangential velocity is measured by a combination of pitot tubes, located at nine radial stations in the midplane ($z/s = 0.5$), and static pressure tappings at the same radii on the stator. A total-temperature probe and pitot tube are also located in a nozzle outlet to measure the temperature and velocity of the inlet flow. More details can be found in Yan et al. [9].

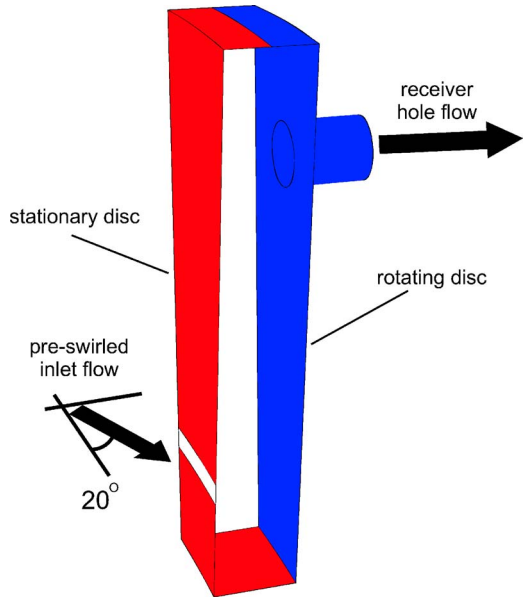

Fig. 2 Schematic diagram of computational domain

The main air supply to the system is passed through a mesh heating element which essentially creates a step change in temperature immediately downstream of the heater; owing to heat losses in the ducting, the temperature rise of the air downstream of the preswirl nozzles is exponential. A strobe light is used to illuminate the rotor and the resulting transient disk temperature distribution is captured on digital video at 25 frames/s. The red–green–blue (RGB) signals of each frame are converted to hue and analyzed to calculate the temperature history and steady-state heat transfer coefficient, as described by Newton et al. [12].

4 Computational Method

The computational domain is designed to be a realistic representation of the experimental rig described above, the only exception being the preswirl nozzles. To enable steady-state computations, the preswirl nozzles are modeled as an axisymmetric slot having the same inlet area, and therefore the same inlet velocity, as the nozzles. The model contains a 1/60th sector of the experimental rig, i.e., a 6 deg section enclosing one of the receiver holes. Boundaries have either a no-slip condition or a periodic interface applied, and walls are defined as rotating or stationary as required. Clearances at no-flow boundaries were taken to be zero.

Figure 2 shows the computational domain, the red shaded areas being stationary while the blue shaded areas rotate with angular velocity Ω. Axial and circumferential velocities are prescribed at the inlet to give the flow angle of 20 deg to the tangential direction. Velocity and static temperature values were prescribed to match measurements made at the nozzle. At the outlet a static pressure boundary condition was used.

The commercial code used for this investigation is CFX5.7, a finite volume, coupled algebraic multigrid solver. The advection scheme is second-order accurate based on the method of Barth and Jesperson [15]. The energy equation is solved, including the viscous work term, and variable density effects taken into account. Buoyancy effects within the wheel space are ignored.

The mesh is a hybrid of unstructured tetrahedral elements, with prismatic elements near the wall. Delaunay triangulation is used to create the surface mesh followed by an advancing front volume mesher. A mesh sensitivity study was carried out to confirm that the fluid dynamics and heat transfer results are not grid dependent. Typical y^+ distributions, for computations both in the viscous and inertial regime, are shown in Fig. 3, and are within the required range for the turbulence model.

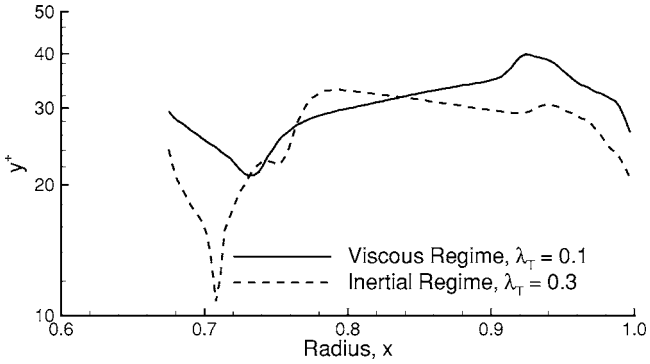

Fig. 3 Typical radial distribution of y^+ on the rotor for inertial and viscous regime computations

The turbulence model used is the high-Reynolds number baseline (BSL) model of Menter [16]. This is a blend of a k-ω formulation with wall functions (Ref. [17]), in the near wall region, and a k-ε model away from the wall. This overcomes sensitivities to freestream turbulence levels normally experienced by k-ω models [18]. The convective heat transfer model applied to the rotor wall is based on the method of Kader [19]; and other surfaces were assumed adiabatic.

Additional computations were performed to confirm that the results were not sensitive to inlet turbulence level or to the uniform rotor temperature boundary condition used to approximate the time varying distribution that occurred in the experiment.

5 Fluid Dynamics

5.1 Velocity and Pressure. Figure 4(*a*) shows a comparison between the computed and measured radial variation of β_∞, the nondimensional swirl ratio at the midplane ($z/s=0.5$). The maximum value of β_∞, which occurs at the inlet radius due to the flow from the nozzles, is well predicted by the computations. However, at the larger radii, the computations overpredict the measured values. This may be due in part to overprediction of turbulence levels by the high-Reynolds number turbulence model.

Figure 4(*b*) shows good agreement between the computed and measured radial distribution of static pressure. In the rotating core of fluid, away from the rotor and stator, $dp/dr=\rho v_\phi^2/r$, and as a consequence the static pressure increases radially. The overprediction of the total pressure in Fig. 4(*c*) is caused mainly by the overprediction of β_∞ referred to above.

The agreement between computations and measurements shown in Fig. 4(*a*) is best for the lowest value of λ_T shown, for which the flow is in the viscous regime. The computed mixing at the higher values of λ_T (for which the flow is in the inertial regime) may be affected by the use of a high-Reynolds-number turbulence model and the simplified slot geometry at inlet. (Yan et al. [9], who used a discrete nozzle inlet and a low-Reynolds-number k-ε turbulence model, obtained better agreement with measurements than that shown in Fig. 4(*a*).)

5.2 Adiabatic Effectiveness. The adiabatic effectiveness, $\Theta_{b,\mathrm{ad}}$, is defined as

$$\Theta_{b,\mathrm{ad}} = \frac{c_p(T_{0,p} - T_{t,b})}{0.5\Omega^2 r_b^2} \tag{7}$$

For given inlet conditions the total temperature of the air in the rotating receiver holes, $T_{t,b}$, decreases linearly as $\Theta_{b,\mathrm{ad}}$ increases.

Karabay et al. [6] derived a theoretical value for $\Theta_{b,\mathrm{ad}}$ using the first law of thermodynamics; the work done on, or by, the air was proportional to the moment required to change the tangential velocity of the air from $\beta_p \Omega r_p$, at the preswirl nozzles, to Ωr_b in the receiver holes. Their equation, which was derived for a *cover-*

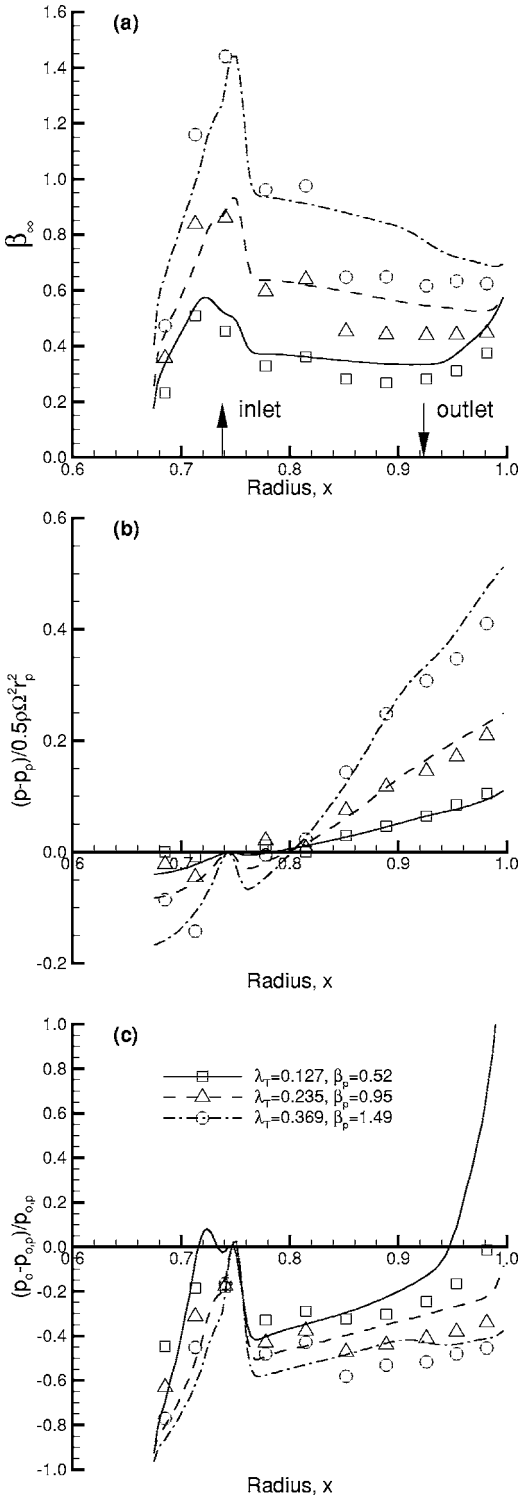

Fig. 4 Comparison of computed (lines) and measured (symbols) results for swirl ratio and pressure: $Re_\phi=0.8\times10^6$

plate system in which there is no stator to reduce the swirl, is given by

$$\Theta_{b,\mathrm{ad}} = 2\beta_p\left(\frac{r_p}{r_b}\right)^2 - 1 \tag{8}$$

It should be noted that $\Theta_{b,\mathrm{ad}} \propto \beta_p$: $\Theta_{b,\mathrm{ad}}$ increases, and $T_{t,b}$ decreases, monotonically with β_p even when $\beta_p > 1$. Karabay et al. also used CFD to compute $\Theta_{b,\mathrm{ad}}$ in a cover-plate system for $0 \leqslant \beta_p \leqslant 3$, and their computations were in good agreement with this equation.

Farzaneh-Gord et al. [5] modified Eq. (8) for a *direct-transfer system* to account for the moment on the stator, M_s. Their model gives

$$\Theta_{b,\mathrm{ad}} = 2\beta_p\left(\frac{r_p}{r_b}\right)^2 - 1 - \frac{M_s}{1/2\dot{m}\Omega r_b^2} \tag{9}$$

where the effect of M_s (a positive quantity) is to reduce $\Theta_{b,\mathrm{ad}}$.

Figure 5(*a*) shows a comparison between the computed and theoretical values of $\Theta_{b,\mathrm{ad}}$ for the present case, where $r_p/r_b=0.8$. The computations based on Eq. (7) use the bulk-average relative total temperature computed at the outlet from the receiver holes. These computations are in excellent agreement with the theoretical values of $\Theta_{b,\mathrm{ad}}$ based on Eq. (9) for the direct-transfer system; the values of M_S in this equation were obtained by computing the tangential shear stress over all of the stationary surfaces in the rig geometry. The theoretical values of $\Theta_{b,\mathrm{ad}}$ calculated using Eq. (8) for a cover-plate system are significantly higher than those for the direct-transfer system.

The theoretical values of $\Theta_{b,\mathrm{ad}}$ are based on the assumption that the air achieves solid-body rotation in the receiver holes. Figure 5(*b*) shows that β_2, the computed bulk-average value of β at the outlet from the holes, is indeed close to unity. (The fact that the computed values of $\beta_2 \approx 1$ could be due to the assumed constant pressure condition at outlet from the receiver holes. In an engine, where the blade-cooling air flows radially outward from the receiver holes, solid-body rotation would be expected to occur; for a rig with short receiver holes, it is possible that solid-body rotation would not be achieved.)

It should be pointed out that both the computed and theoretical values of $\Theta_{b,\mathrm{ad}}$ for the direct-transfer rig depend, explicitly or implicitly, on the computed value of M_s. It is, therefore, uncertain that the theory will agree with experimental measurements of $\Theta_{b,\mathrm{ad}}$, which were not made in the tests reported here. The measurement of $\Theta_{b,\mathrm{ad}}$ is nontrivial: the actual (not the isentropic) value of β_p must be known; the bulk-average relative velocity and total temperature inside the receiver holes must be measured accurately; and the rotating disk should be made from a thermal insulator to reduce the heat transfer to the cooling air. These three conditions are seldom, if ever, achieved in rotating-disk rigs.

5.3 Discharge Coefficients. So as to be consistent with other research workers, the discharge coefficient for the receiver holes is defined as

$$C_D = \frac{\dot{m}_b}{\dot{m}_i} \tag{10}$$

where $\dot{m}_i$ is the isentropic mass flow rate. This can be calculated from the first law of thermodynamics, for an adiabatic system, taking into account the rate of work done by or on the air from Stations 1–2 in a stream tube. The equation derived by Yan et al. [9] is

$$\frac{\dot{m}_i}{A_2} = \rho_{0,1}\left(\frac{p_2}{p_{0,1}}\right)^{1/\gamma}\left\{\left(\frac{2\gamma}{\gamma-1}\right)\frac{p_{0,1}}{\rho_{0,1}}\left[1-\left(\frac{p_2}{p_{0,1}}\right)^{\gamma-1/\gamma}\right] + 2\Omega(r_2V_{\phi,2} - r_1V_{\phi,1}) - V_{\phi,2}^2\right\}^{1/2} \tag{11}$$

The first term inside the curly brackets is the standard result for compressible flow in a stationary nozzle; the second term is the work term resulting from the change of angular momentum of the air; the last term is due to the fact that the air in the receiver holes has an absolute tangential, as well as an axial, component of velocity. In their measurements, Yan et al. based $p_{0,1}$ and $V_{\phi,1}$ on their pitot-tube measurements at $r=r_b$ and $z/s=0.5$. They took p_2

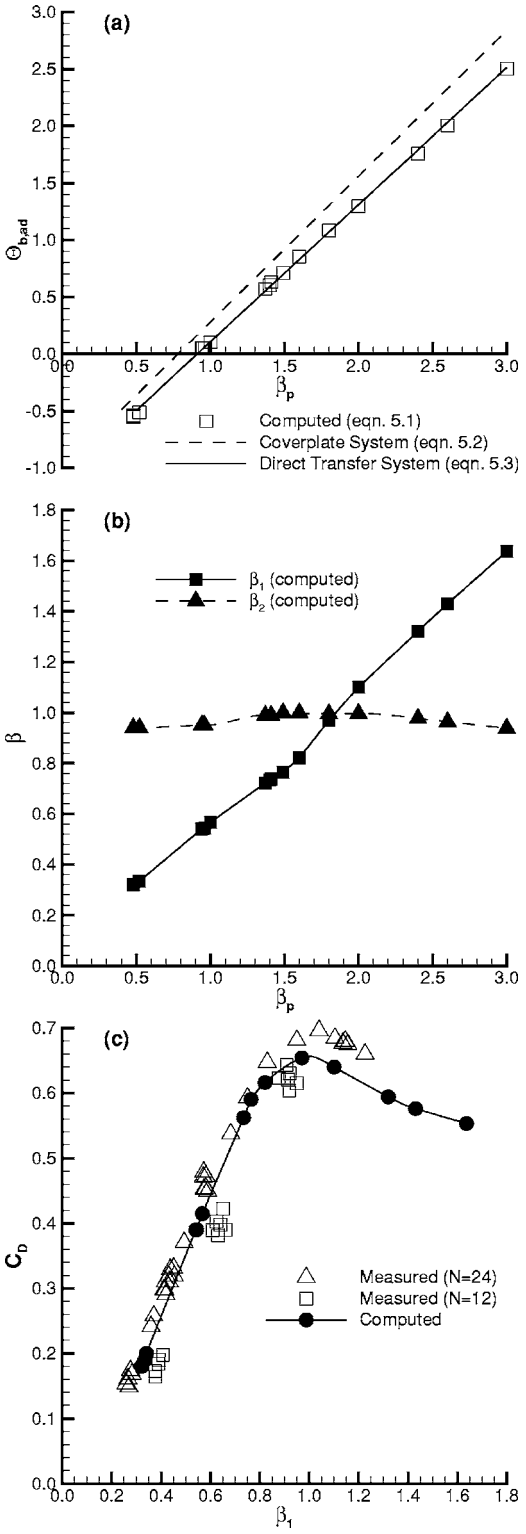

Fig. 5 Variation of $\Theta_{b,ad}$, β, and C_D with β_p for $0.8\times10^6<\mathrm{Re}_\phi<1.2\times10^6$ and $0.12<\lambda_T<0.38$: (*a*) comparison between computed and theoretical $\Theta_{b,ad}$; (*b*) comparison between computed β_1 and β_2; and (*c*) comparison between computed and measured C_D

as the atmospheric pressure at outlet from the receiver holes, and assumed that $V_{\phi,2}=\Omega r_b$. The same assumptions and locations were used here in determining the computed values of $\dot{m}_i$.

As shown in Fig. 5(*b*) the computed values of β_2 are close to unity, supporting the assumption of solid-body rotation at the outlet from the receiver holes. The computed values of β_1, which are based on the bulk-average values of $V_{\phi,1}$ calculated at $r=r_1=r_b$ and $z/s=0.5$, are significantly smaller than β_p, and it should be noted that $\beta_1=1$ when $\beta_p\approx1.8$.

Figure 5(*c*) shows a comparison between the computed and measured variation of C_D with β_1. The measured values were obtained with 24 and 12 preswirl nozzles ($N=24$ and $N=12$); the $N=12$ results were obtained by blocking alternate nozzles. As for all computations presented in this paper, the computed results were obtained for the case where the annular slot in the stator had an area equivalent to the $N=24$ tests.

As expected, the computations and experiments show that C_D reaches a maximum value at $\beta_1=1$; the computed maximum of $C_D=0.65$ is lower than that in the experiments, $C_D=0.70$. Dittman et al. [20] measured discharge coefficients for a rotating short orifice, with the same length to diameter ratio as the receiver holes, and found that C_D had a maximum value of 0.78 when the fluid and the orifice had the same circumferential velocity.

The maximum value of C_D occurs at a critical value of β_p, which will depend strongly on the system geometry. For the system used here, the critical value of β_p was approximately 1.8 for the computations and 2.3 for the experiments. The important practical consequence is that, although the cooling effectiveness increases monotonically as β_p increases, the flow rate of the blade cooling air will decrease if the critical value of β_p is exceeded.

6 Heat Transfer

6.1 Radial Variation of Nusselt Number. The computed heat flux is nondimensionalised to form the local Nusselt number, Eq. (13), based on the adiabatic disc temperature derived by Karabay et al. [6] for a cover-plate system and which is shown in Eq. (12)

$$T_{w,\mathrm{ad}}=T_{0,p}-\frac{V_{\phi,\infty}^2}{2C_p}+R\frac{\Omega^2r^2}{2C_p}\left(1-\frac{V_{\phi,\infty}}{\Omega r}\right)^2 \tag{12}$$

$$\mathrm{Nu}=\frac{q_w r}{k(T_w-T_{w,\mathrm{ad}})} \tag{13}$$

Equation (12) is a theoretical value based on the Reynolds analogy, and the values of $T_{w,\mathrm{ad}}$ computed by Karabay et al. [6] were in excellent agreement with this equation. Newton et al. [12] used wide-band TLC to measure the adiabatic-disk temperature on the Bath rig. Apart from the region near the preswirl nozzles, the differences between the measured and theoretical values of $T_{w,\mathrm{ad}}$ were mostly less than 0.5°C. Owing to the uncertainty in the wide-band TLC measurements, Eq. (12) was used to calculate $T_{w,\mathrm{ad}}$ for the measured Nusselt numbers.

Owen and Rogers [21] showed that, for turbulent boundary-layer flow in rotor-stator systems, $\mathrm{Nu}\propto\mathrm{Re}_\phi^{0.8}$. If the heat transfer in the Bath rig is controlled by turbulent boundary-layer flow then the parameter $\mathrm{Nu}\,\mathrm{Re}_\phi^{-0.8}$ would be expected to be independent of Re_ϕ.

Figure 6 shows a comparison between computed and experimental values of $\mathrm{Nu}\,\mathrm{Re}_\phi^{-0.8}$ for three values of λ_T and three values of Re_ϕ (As Eq. (5) shows, $\beta_p\propto\lambda_T$). The measured local Nusselt numbers were obtained by Lock et al. [13], and those shown in Fig. 6 were evaluated along a radial line midway between two adjacent receiver holes.

Figure 6(*a*), for $\lambda_T=0.13$ and $\beta_p=0.5$, shows a distinct peak in heat transfer near the receiver holes ($x=0.93$) but there is no sign of impingement near the preswirl nozzles ($x=0.74$). Lock et al. defined this as the viscous regime, and it can be seen that $\mathrm{Nu}\,\mathrm{Re}_\phi^{-0.8}$ is a good correlating parameter for both the computational and experimental results. Although the radial variation of the computations and measurements are qualitatively similar, the compu-

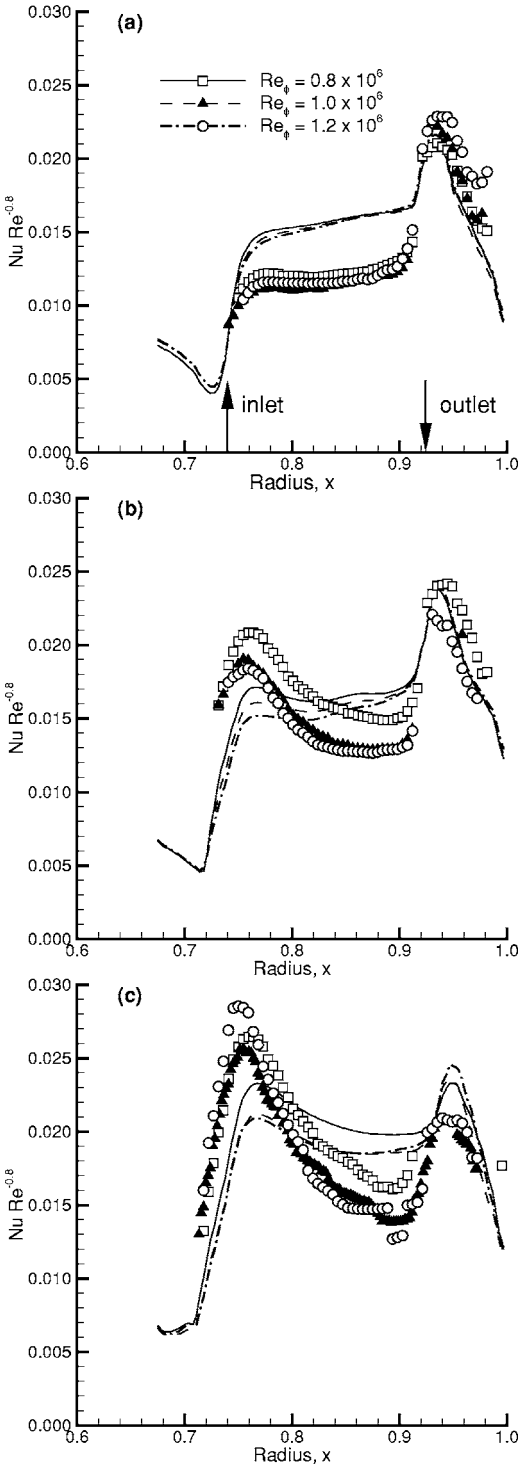

Fig. 6 Radial variation of Nu $Re_\phi^{-0.8}$: (*a*) λ_T=0.12, β_p=0.5; (*b*) λ_T=0.24, β_p=1.0; and (*c*) λ_T=0.35, β_p=1.5

tations overpredict the measured values except in the region near the receiver holes.

In Fig. 6(*b*) for $\lambda_T \approx 0.24$ and $\beta_p \approx 1.0$, the experimental results show a distinct peak near the nozzles, signifying that the flow is in the inertial regime. The computations show only a small peak at this radius. For these conditions, the parameter Nu $Re_\phi^{-0.8}$ fails to collapse either the experimental or computational data.

In Fig. 6(*c*) for $\lambda_T \approx 0.35$ and $\beta_p \approx 1.5$, both sets of results exhibit the inertial peak near the preswirl nozzles. The radial variation of the computations and measurements are qualitatively similar, but again the parameter Nu $Re_\phi^{-0.8}$ fails to collapse the data.

6.2 Circumferential Variation of Nusselt Number. Figure 7 shows comparisons of Nusselt number contours across an 18 deg sector of the rotor, as studied experimentally. Results on the right were produced by computation and those on the left are experimental results. The conditions for case 7(*a*) classify it within the viscous regime; the two other examples, 7(*b*) and 7(*c*), relate to the inertial regime.

Comparing Fig. 7(*a*) with the results in Fig. 6, the same difference in Nusselt number magnitude is visible and the improved agreement at the receiver hole radius is also apparent. In the region close to the edge of the holes there is an absence of experimental data caused by the presence of the Rohacell bushes described in Sec. 3. (The opaque bushes also cause shadows over the transparent rotor, obscuring the results in this region.)

In Fig. 7(*b*) and 7(*c*), representing the inertial regime, there is good qualitative agreement between computations and measurements at high radii.

A small region of high heat transfer is observable around the receiver holes in each case in Fig. 7. At low λ_T and β_p this region is located at the "9 o'clock position" with respect to the holes, Fig. 7(*a*). As λ_T and β_p are increased the region moves around towards the "11 o'clock position," Fig. 7(*c*). Luo et al. [22] performed temperature measurements around a rotating disk with receiver holes and observed similar behavior around the holes. (In an engine, high heat transfer in this region could result in thermal stresses within the rotor.)

6.3 Physical Interpretation of Heat Transfer Results. Using an axisymmetric CFD code, Wilson et al. [11] showed that air entered the receiver holes by "direct" and "indirect" routes. The former refers to flow traveling directly along a streamline connecting the inlet and the outlet, and therefore not mixing with the core flow. Indirect flow mixes with the core flow before entering the receiver holes.

This idea can be extended to the study of nonaxisymmetric systems by considering that the direct flow travels in a stream tube between the preswirl nozzles and the receiver holes. Computing streamlines for the direct flow allows the path of the stream tube to be evaluated. Figure 8 shows the stream tube relative to the rotor for a variety of conditions. The inner location is at the radius of the preswirl nozzles, and the outer location is at the radius of the receiver holes. These results show only a weak effect of Re_ϕ.

Figure 9 shows measured heat transfer results combined with streamlines calculated using the *full* velocity field from the computations. Figure 9(*a*) is a radial section with the preswirl inlet and stator on the left and the receiver hole and rotor on the right. The orange streamline shows that flow from the nozzle can be either direct or indirect: the direct flow exits through the receiver hole; the indirect flow continues to a higher radius and will recirculate in the system and mix with the core flow. The black streamline shows that indirect flow, which has entered the core, can either exit through the receiver hole or continue circulating in the core.

Figure 9(*b*) shows the same streamlines in a circumferential section. It can be seen that the flow at the rotor surface that is aligned with the receiver holes becomes direct flow. The remaining flow follows the indirect route.

Figure 9(*c*) shows an isometric view of the same streamlines. It is the flow from the core, replacing the boundary layer flow entering the receiver holes, which gives rise to the region of high heat transfer.

7 Conclusions

Flow and heat transfer measurements from an experimental study of a preswirl rotor–stator system have been compared with the results of computations. The experiments were conducted on

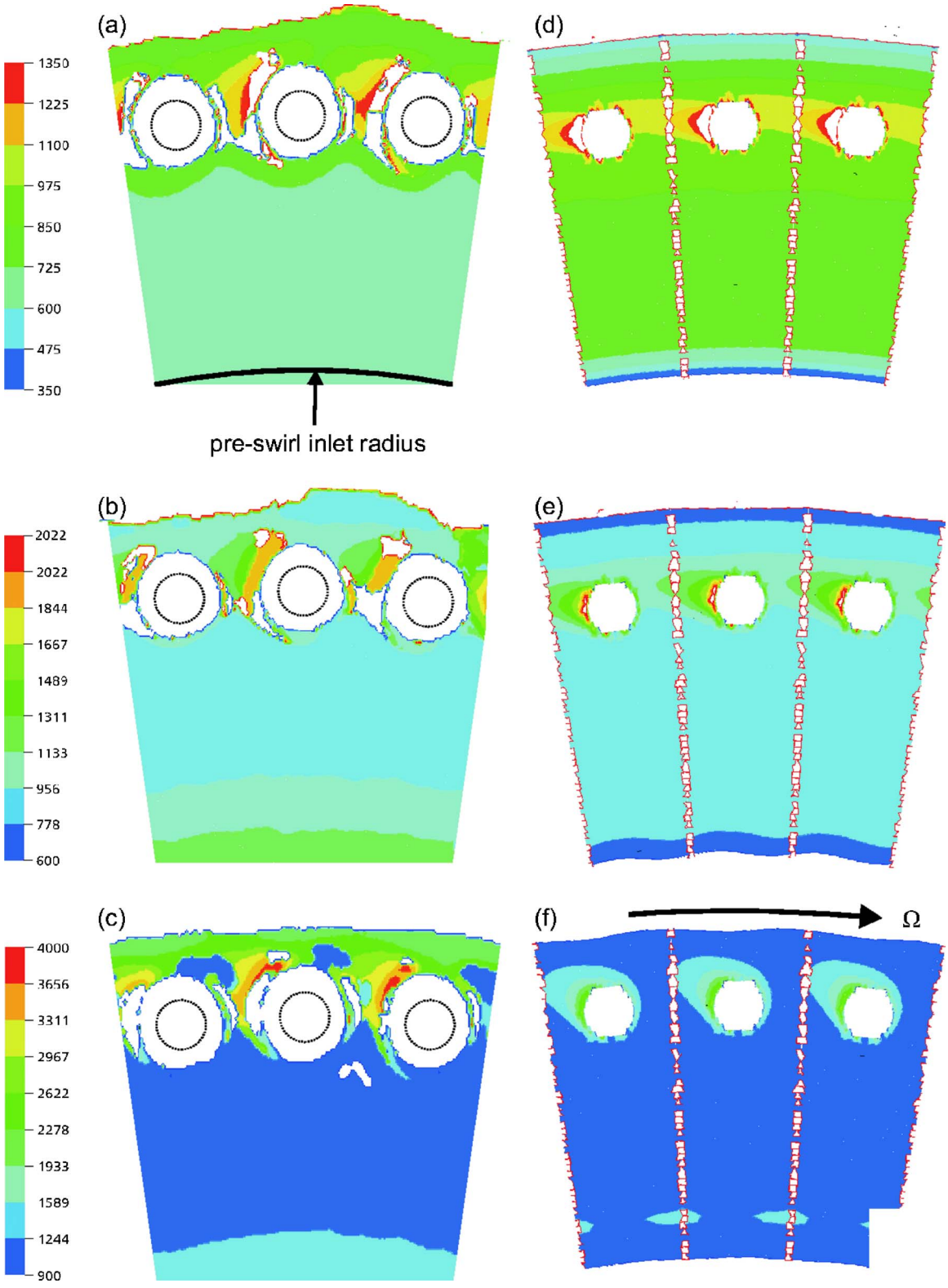

Fig. 7 Experimental (left) and computational (right) Nusselt number contours, $Re_\phi = 0.8 \times 10^6$: (a) $\beta_p = 0.5$, $\lambda_T = 0.13$; (*b*) $\beta_p = 1.0$, $\lambda_T = 0.24$; and (*c*) $\beta_p = 1.5$, $\lambda_T = 0.37$

the "Bath rig:" a purpose-built direct-transfer rig. The measurements were made for $0.8 \times 10^6 < Re_\phi < 1.2 \times 10^6$, $0.1 < \lambda_T < 0.4$ and $0.5 < \beta_p < 1.5$, and the flow structure was considered to be representative of that found in gas turbines. The steady-state computations used a 3D commercial CFD code.

The conclusions based on this rig geometry are as follows:

1. The computed static pressure distribution agrees well with measured values but the tangential velocity, and hence the total pressure, is overpredicted.

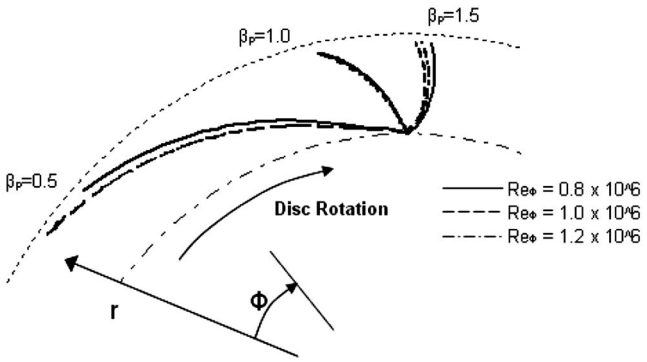

Fig. 8 Streamline plots for flow in the direct route between inlet and outlet

2. The computed values of $\Theta_{b,\mathrm{ad}}$ were in good agreement with a theoretical model for direct-transfer systems.
3. The discharge coefficient, C_D, reached a maximum value when β_1, the core swirl ratio adjacent to the receiver holes, was unity. The computed maximum was $C_D \approx 0.65$, and the experimental maximum was $C_D \approx 0.70$.
4. The computed and measured radial distributions of Nusselt number, Nu, on the rotating disk show evidence of the viscous and inertial regimes. Although Nu tends to increase as Re_ϕ increases, the parameter $\mathrm{Nu}\,\mathrm{Re}_\phi^{-0.8}$ is only weakly dependent on Re_ϕ in the viscous regime. The computations are qualitatively similar to the measurements but, apart from the region near the receiver holes, they do not show good quantitative agreement.
5. The computed and measured contours of Nu show that there is a small region of high heat transfer close to the receiver holes. This is due to the two routes by which flow enters the holes: a "direct" route from the preswirl nozzles and an "indirect" route from the core. The regions of high heat transfer are of importance for designers as they may result in thermal stresses around the receiver holes in turbine disks.

Acknowledgment

Paul Lewis is a Ph.D. student funded by the UK Engineering and Physical Sciences Research Council (EPSRC) through a Doctoral Training Account (DTA). The experimental work was performed by Dr Y. Yan, who was funded by Alstom Power Ltd (now Siemens Industrial Turbines) and EPSRC, and additional discharge coefficient measurements were made by Vinod Kakade from the University of Bath. The authors would like to thank the reviewers for their constructive feedback during the review process.

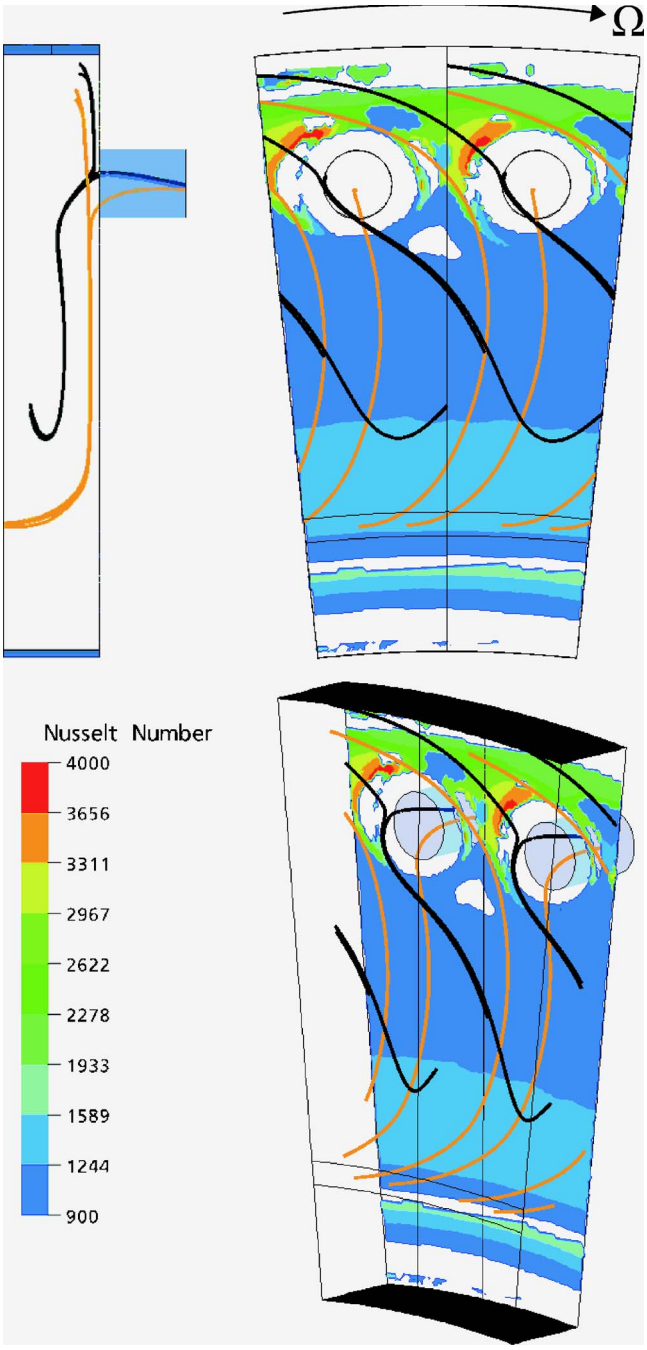

Fig. 9 Computed streamlines superimposed onto experimental heat transfer results: $\mathrm{Re}_\phi = 0.8 \times 10^6$, $\beta_p = 1.5$, $\lambda_T = 0.38$

Nomenclature

a = rotor inner radius
b = rotor outer radius
c_p = specific heat capacity at constant pressure
c_w = nondimensional mass flow rate ($=\dot{m}/\mu b$)
C_D = discharge coefficient for receiver holes
d = preswirl nozzle diameter
G = gap ratio ($=s/b$)
h = heat transfer coefficient
k = thermal conductivity of air
$\dot{m}$ = mass flow rate
M = disk moment
N = number of preswirl nozzles
Nu = Nusselt number ($=q_w r/k(T_w - T_{w,\mathrm{ad}})$)
Pr = Prandtl number ($=\mu c_p/k$)
q_w = rotor wall heat flux
R = recovery factor ($=\mathrm{Pr}^{1/3}$)
Re_ϕ = rotational Reynolds number ($=\rho\Omega b^2/\mu$)
r = radius
r_p, r_b = radii of preswirl nozzles and receiver holes
s = rotor–stator separation distance
T = static temperature
v = velocity
u_τ = friction velocity
x = nondimensional radius ($=r/b$)
y = distance normal to the wall
y^+ = nondimensional wall distance ($=\rho y u_\tau/\mu$)
β = swirl ratio ($=v_\phi/\Omega r$)
γ = ratio of specific heats

$\Theta_{b,\mathrm{ad}}$ = adiabatic effectiveness
λ_T = turbulent flow parameter ($=c_w \mathrm{Re}_\phi^{-0.8}$)
μ = dynamic viscosity
ρ = density
Ω = angular velocity of rotor

Subscripts

ad = adiabatic
b = blade-cooling
i = isentropic value
o = total value in stationary frame
p = preswirl
s = stator
t = total value in rotating frame
w = rotor
ϕ, r, z = circumferential, radial, axial direction
∞ = value in core at $z/s=0.5$
1,2 = upstream, downstream locations in a stream tube

References

[1] Meierhofer, B., and Franklin, C. J., 1981, "An Investigation of a Preswirled Cooling Airflow to a Turbine Disc by Measuring the Air Temperature in the Rotating Channels," ASME Paper 81-GT-132.

[2] El-Oun, Z. B., and Owen, J. M., 1989, "Preswirl Blade-Cooling Effectiveness in an Adiabatic Rotor-Stator System," ASME J. Turbomach., **111**, pp. 522–529.

[3] Geis, T., Dittmann, M., and Dullenkopf, K., 2003, "Cooling Air Temperature Reduction in a Direct Transfer Preswirl System," ASME Paper GT2003-38231.

[4] Chew, J. W., Ciampoli, F., Hills, N. J., and Scanlon, T., 2005, "Pre-Swirled Cooling Air Delivery System Performance," ASME Paper GT2005-68323.

[5] Farzaneh-Gord, M., Wilson, M., and Owen, J. M., 2005, "Numerical and Theoretical Study of Flow and Heat Transfer in a Pre-Swirl Rotor-Stator System," ASME Paper GT2005-68135.

[6] Karabay, H., Wilson, M., and Owen, J. M., 2001, "Predictions of Effect of Swirl on Flow and Heat Transfer in a Rotating Cavity," Int. J. Heat Fluid Flow, **22**, pp. 143–155.

[7] Popp, O., Zimmermann, H., and Kutz, J., 1998, "CFD Analysis of Coverplate Receiver Flow," ASME J. Turbomach., **120**, pp. 43–49.

[8] Dittmann, M., Geis, T., Schramm, V., Kim, S., and Wittig, S., 2002, "Discharge Coefficients of a Preswirl System in Secondary Air Systems," ASME J. Turbomach., **124**, pp. 119–124.

[9] Yan, Y., Farzaneh-Gord, M., Lock, G., Wilson, M., and Owen, J. M., 2003, "Fluid Dynamics of a Pre-Swirl Rotor-Stator System," ASME J. Turbomach., **125**, pp. 641–647.

[10] Lock, G. D., Wilson, M., and Owen, J. M., 2005, "Influence of Fluid Dynamics on Heat Transfer in a Pre-Swirl Rotating Disc System," ASME J. Eng. Gas Turbines Power, **127**, pp. 791–797.

[11] Wilson, M., Pilbrow, R., and Owen, J. M., 1997, "Flow and Heat Transfer in a Pre-Swirl Rotor-Stator System," ASME J. Turbomach., **119**, pp. 364–373.

[12] Newton, P. J., Yan, Y., Stevens, N. E., Evatt, S. T., Lock, G. D., and Owen, J. M., 2003, "Transient Heat Transfer Measurements Using Thermochromic Liquid Crystal. Part 1: An Improved Technique," Int. J. Heat Fluid Flow, **24**, pp. 14–22.

[13] Lock, G. D., Yan, Y., Newton, P. J., Wilson, M., and Owen, J. M., 2005, "Heat Transfer Measurements Using Liquid Crystals in a Preswirl Rotating-Disk System," ASME J. Eng. Gas Turbines Power, **127**, pp. 375–382.

[14] Owen, J. M., and Rogers, R. H., 1995, *Flow and Heat Transfer in Rotating-Disc Systems* (Vol. 2, Rotating Cavities), Research Studies Press, Taunton, UK.

[15] Barth, T. J., and Jesperson, D. C., 1989, "The Design and Application of Upwind Schemes on Unstructured Meshes," *Proc. 27th AIAA Aerospace Sciences Meeting*, Reno, NV, January 9–12.

[16] Menter, F. R., 1994, "Two-Equation Eddy Viscosity Turbulence Models for Engineering Applications," AIAA J., **32**(8), pp. 269–289.

[17] Wilcox, D. C., 1998, *Turbulence Modelling for CFD*, 2nd ed., DCW Industries, La Canada, CA.

[18] Ansys Inc., "CFX User Documentation," Version 5.7, Ansys, Inc., Canonsburg, PA.

[19] Kader, B. A., 1981, "Temperature and Concentration Profiles in Fully Turbulent Boundary Layers," Int. J. Heat Mass Transfer, **24**(9), pp. 1541–1544.

[20] Dittmann, M., Dullenkopf, K., and Wittig, S., 2004, "Discharge Coefficients of Rotating Short Orifices With Radiused and Chamfered Inlets," ASME J. Eng. Gas Turbines Power, **126**, pp. 803–808.

[21] Owen, J. M., and Rogers, R. H., 1989, "Flow and Heat Transfer in Rotating-Disc Systems," *Rotor-Stator Systems*, Research Studies Press, Taunton, UK, Vol. 10.

[22] Luo, X., Zhang, C., Xu, G., Tao, Z., and Ding, S., 2004, "Measurements of Surface Temperature Distribution on a Rotating Disk With Blade Cooling Holes Using Thermochromic Liquid Crystal," ASME Paper GT2004-53519.